Quantum Chemical Molecular Dynamics Simulations of Dynamic Fullerene Self-Assembly in Benzene Combustion

Biswajit Saha,[†] Sho Shindo,[†] Stephan Irle,[†,‡,*] and Keiji Morokuma[†,*]

[†]Fukui Institute for Fundamental Chemistry, Kyoto University, Kyoto, 606-8103, Japan, and [‡]Institute for Advanced Research and Department of Chemistry, Nagoya University, Nagoya 464-8602, Japan

ARTICLE

ABSTRACT Using density-functional tight-binding (DFTB)-based quantum chemical molecular dynamics at 2500 and 3000 K, we have performed simulations of benzene combustion by gradually reducing the hydrogen to carbon (H/C) ratio. The accuracy of DFTB for these simulations was found to be on the order of 7—9 kcal/mol when compared to higher-level B3LYP and G3-like quantum chemical methods in extensive benchmark calculations. Ninety direct-dynamics trajectories were run for up to 225 ps simulation time, during which hydrocarbon cluster size, curvature, and C_xH_y composition, carbon hybridization type, and ring count statistics were recorded. Giant fullerene cage formation was observed only after hydrogen was completely eliminated from the reaction mixture, with yields of around 50% at 2500 K and 42% at 3000 K. Cage sizes are mostly in the range from 152 to 202 carbon atoms, with the distribution shifting toward larger cages at lower temperature. In contrast to previous simulations of dynamics fullerene assembly from ensembles of C_2 molecules, we find that the resulting cages show smaller number of attached carbon chains (antenna) surviving until cage closure. Again, no direct formation pathway for C_{60} from smaller fragments was observed. Our results challenge the idealized picture of "ordered" growth of PAHs along a route involving only maximally condensed and fully hydrogenated graphene platelets, and favor instead fleeting open-chains with ring structures attached, featuring a large number of hydrogen defects, pentagons, and other nonhexagon ring species.

KEYWORDS: quantum chemical molecular dynamics simulations · density-functional tight-binding · dynamic self-assembly · fullerene formation · benzene combustion · H/C ratio change during combustion · nonequilibrium dynamics

Fullerenes were traditionally synthesized by evaporation of carbon from graphite at very high temperatures on the order of several thousand degrees Celsius.[1,2] Nowadays, the fascinating sp^2 carbon cages are industrially produced using fuel-rich hydrocarbon flames diluted with argon and burning in lean oxygen sooting flames at temperatures up to 2000 °C.[3−6] While the combustion synthesis offers advantages for large-scale operation, it is sensitive to changes in operating conditions, such as fuel type,[6] fuel/oxygen ratio, temperature, residence time, and chamber pressure[4,5] or even chamber design (spherical burner offers advantages over flat burner).[7] Despite considerable advances in optimizing the conditions,[8] the elementary reaction mechanisms involved in the growth of polycyclic aromatic hydrocarbons (PAHs)[9] and subsequent self-assembly of the fullerene cages[10] are still subject to speculation.

For fullerene formation in carbon-only plasma and vapors, our "shrinking hot giant" (SHG) road of fullerene formation[11−15] including its recent variation by Curl and coworkers[16] provides the most straightforward explanation for the outstanding abundances of C_{60} and C_{70} fullerenes, which emerge in this mechanism as the smallest possible isolated pentagon rule (IPR)-obeying survivors of a grueling giant fullerene (GF, C_n with $n > \sim 90$) cage shrinking process. The SHG mechanism starts with the self-assembly of GFs (termed "size-up") from small gas phase carbon vapor molecules *via* the following three stages: (1) polyyne chain formation (σ-bond formation between small linear carbon chain fragments) and nucleation of a pentagon/hexagon network (sp to sp^2 rehybridization), (2) ring condensation growth (change in carbon hybridization from sp to sp^2, facilitated by growth of polyyne chains attached to the growing network nucleus), and (3) GF cage closure (saturation of dangling bonds at edges).[11,12] The giant cage self-assembly is then followed by irreversible C_2 evaporation from transient large hole areas of the vibrationally excited, highly irregular, and defective GF cages (termed "size-down").[15] The shrinking of GFs and the increase in cage sphericity was recently experimentally followed by HRTEM.[17,18] Clearly, the combined "size-up/size-down" process stands in remarkable contrast to the traditional theories of fullerene formation,[10,19] as well as tight-binding MD simulations[20] of sequential and "orchestrated"[21] C_{10} collisions, which aim to explain direct

*Address correspondence to sirle@iar.nagoya-u.ac.jp, morokuma@fukui.kyoto-u.ac.jp.

Received for review November 6, 2008 and accepted July 16, 2009.

Published online July 31, 2009.
10.1021/nn900494s CCC: $40.75

formation of buckminsterfullerene C_{60} from smaller fragments. However, it is also clear that C_{60} can only form directly from smaller fragments if only sixty carbon atoms are present, and that larger cages naturally emerge if more carbon is added in simulations of the dynamic self-assembly process.[22] From a purely thermodynamic point of view it is counterintuitive that the unusually large yield of buckminsterfullerene $^{Ih}C_{60}$ formation should be the result of an irreversible shrinking process, as larger fullerenes possess larger binding energies per carbon atom than smaller ones.[23] However, we recognize that the shrinking occurs under conditions far from equilibrium conditions where carrier gas pressure and carbon density is gradually decreasing in the expanding laser plume or combustion flame.

We formulated the SHG road of fullerene formation based on the results of quantum chemical molecular dynamics (QM/MD) simulations of carbon-only systems initially consisting of ensembles of C_2 molecules at 2000 K and higher temperatures, considering varying carbon densities. The underlying quantum chemical potential energy was computed in direct-dynamics simulations on the fly using the density-functional tight-binding (DFTB) method.[24,25] This more sophisticated Extended Hückel-like method has passed several benchmark tests with first principle density functional theory (DFT)[24,26] and Møller−Plesset second order perturbation theory[27] for carbon-only systems, and has become well-established as a computationally inexpensive yet reliable quantum chemical level of theory for carbon clusters and fullerenes. Explicit consideration of electronic structure, such as π-conjugation, aromaticity, and delocalization stabilization, is important for the dynamics of carbon cluster systems and is well described by DFTB.[28,29] Computationally more inexpensive classical approaches, such as the reactive bond order (REBO)-type molecular force fields[30−32] are not adequate for the investigation of the fullerene formation mechanism. They predict entirely different fullerene self-assembly mechanisms without the involvement of polyyne chains.[33] In contrast, the size-up mechanism has been confirmed by QM/MD simulations of other research groups.[22,34]

Experimentally, oxygen-lean combustion of hydrocarbon fuels produces substantial amounts of PAHs that have high probability of incorporation into growing fullerenes as they near completion.[5,8,10,35−38] During this process, the presence of hydrogen was found to dramatically slow down the condensation and carbon sheet bending process.[8] But experimental techniques to study the fullerene formation process are usually limited to the simple determination of temperature profile and C/O mole fractions as functions of the distance from the burner head, *in situ* mass spectrometry yielding indirect information on the H/C ratio of PAHs, and combination of these data with thermodynamic considerations and kinetic modeling. Although it is obvious from these studies that PAH molecules grow into soot and fullerenes, no clear identification can be made as to the exact chemical composition of the intermediates: Do they all consist of sp^2-carbon species or are linear sp polyyne species present? When and where do hydrogen abstractions occur, and what are the concentrations and lifetimes for the resulting PAH radical species? How many (if any) pentagons are incorporated in the growing structures? Answers to these questions have been sought before, and for instance Homann and co-workers meticulously recorded the H/C ratio of PAH species for acetylene flames as a function of the burner distance. The recorded C_xH_y species were found to cluster along a "band of growth" with the stoichiometry of its members coinciding with PAH molecules that possess a maximum number of condensed rings and are therefore clearly thermodynamically very stable. The growing PAH platelets should therefore have little to no pentagons, and little hydrogen addition- or loss-defects.[10] However, such a proposal for intermediate structures is hard to reconcile with the fact that soot particles are always curved[5] and that fullerenes require the presence of 12 pentagons. Clearly, H/C ratios in PAHs based on *in situ* mass spectroscopy cannot give *direct* information regarding the carbon skeleton of the high-temperature species, and "rationalization" efforts such as those presented by Homann and co-workers tend to be limited to the thermodynamically most reasonable structures that might emerge after edge saturation with hydrogen and extensive annealing before detection in the mass spectrometer. There is no proof available that the thermodynamically most stable species are really the ones involved in the dynamic self-assembly process. We believe that it is necessary to consider cluster growth as occurring under nonequilibrium conditions at high temperatures under the influence of large temperature and pressure gradients bringing about irreversible processes upon which the dynamic self-assembly phenomenon relies.

Theoretical modeling of combustion PAH growth elementary processes have either stopped at systems around the size of the indene $C_{10}H_{11}$ molecule,[39−41] in the case of highly accurate quantum chemical reaction pathway studies or used poorly connected multiscale techniques which did not demonstrate any fullerene formation due to the small size of the quantum regions considered.[42] PAH formation during benzene combustion was also studied using conventional kinetic models.[43−45] In kinetic modeling, temperature and mole fraction profiles of reactants, products, and intermediates are fed into assumed reaction pathways, where reaction rates are calculated on the basis of transition state theory. Because of the very nature of kinetic modeling, one can only discriminate between the pathways that were "input" in the modeling, and alternative pathways can easily be overlooked. A fully quantum chemical molecular dynamics simulation of

the combustion process in analogy of our previous non-equilibrium high-temperature pure carbon simulations seems therefore desirable. However, a brute force approach that would consider both fuel and O_2 molecules as reaction system is hampered by the fact that H abstraction reactions occur too slow[46] even for reactive classical force field (ReaxFF) MD simulations.[47] Our own preliminary calculations with benzene molecules mixed with oxygen molecules indicate that the removal of hydrogen atoms or other possible reactions do not occur on the order of tens of picoseconds. At the same time, it is clear that oxidation will eventually lead to the exothermic products H_2O, CO, and CO_2, driving the combustion and injecting thermal energy, but otherwise these are nonreactive closed-shell molecules not expected to participate in the PAH growth process. Hence, in this work, we gradually lowered the H/C ratio as described below during constant temperature QM/MD simulations of systems initially consisting of 36 benzene molecules.

The findings of our study are presented in the "Results" section as follows: After demonstrating the validity of DFTB for PAH combustion chemistry by benchmarking against first principles hybrid DFT (B3LYP) and *ab initio* G3-type data, we discuss the formation rate, structural composition, size, and yield of the GFs formed in "successful" trajectories. We then follow the trajectories in more detail, describing radical initiation reactions, and discuss the time dependence of cluster size, H/C composition and carbon sp^n hybridization of C_xH_y fragments as well as the number of carbon-skeleton pentagons/hexagons/heptagons during the simulated benzene combustion. These data are related to the H/C ratio present in the system. In the "Discussion" section, we describe in greater detail the mechanism of fullerene formation during PAH combustion as observed in our simulations and attempt to connect our data to available experimental results.

RESULTS

DFTB Benchmark. To ensure that DFTB accurately reproduces geometries and energetics of hydrocarbon radical species, we have used the B3LYP/6-311G** and G3(MP2,CC)//B3LYP/6-311G** results reported by Kislov et al.[41] for reaction barrier heights and relative energies of possible pathways of indene C_9H_8 formation from cyclopentadiene and the cylcopentadienly radical, and compared them with both noncharge-consistent (NCC) and self-consistent-charge (SCC) versions of DFTB after reoptimization of the structures at the respective level. Table 1 summarizes respective rmsd and R^2 values for the 145 species, and we find that NCC-DFTB and SCC-DFTB give an overall rmsd energy deviation from B3LYP/6-311G** of 7.10 and 6.62 kcal/mol, respectively, with linear regression R^2 values of 0.926 (NCC) and 0.945 (SCC). The systematic error is small since linear regression slopes are close to 1.0 with

TABLE 1. The rmsd in [kcal/mol] and Overall R^2 Values for NCC- and SCC-DFTB 87 Barrier Heights and 58 Reactant, Intermediate, and Product Energies Compared to B3LYP/6-311G and G3(MP2/CC) Data Reported by Kislov *et al.* (ref 41) in Their Study of Possible Pathways of Indene C_9H_8 Formation from Cyclopentadiene and the Cylcopentadienly Radical**

	B3LYP		G3(MP2/CC)		
	NCC-DFTB	SCC-DFTB	NCC-DFTB	SCC-DFTB	B3LYP
barrier heights	6.58	6.09	7.07	7.15	5.15
minima	7.74	7.21	10.82	10.42	5.13
overall rmsd	7.10	6.62	8.87	8.70	5.11
overall R^2	0.926	0.945	0.902	0.926	0.983

0.968 and 0.996 for NCC- and SCC-DFTB, respectively (see Figures S1 and S2 in the Supporting Information, which also lists the entire set of data in Tables S1 and S2). Compared to the more accurate G3(MP2,CC)//B3LYP/6-311G** data, NCC-DFTB and SCC-DFTB give a slightly worse overall rmsd energy deviation of 8.87 and 8.70 kcal/mol, respectively, with linear regression R^2 values of 0.902 (NCC) and 0.926 (SCC). The systematic error this time is larger since linear regression slopes deviate more from 1.0 with 1.062 and 1.091 for NCC- and SCC-DFTB, respectively (see Figures S3 and S4 in the Supporting Information and corresponding Tables S3 and S4). For comparison, B3LYP/6-311G** has a deviation of 5.11 kcal/mol for heat of reactions from the highly accurate G3(MP2,CC)//B3LYP level of theory, a slope of 1.103 (see Figure S5), and a linear regression R^2 value of 0.983. We note that the NCC-DFTB and SCC-DFTB energies and consequently relative energies and barrier heights are rather close, since the charge polarization in these systems is generally small. The similarity of the DFTB energetics to the B3LYP and G3(MP2,CC) data is remarkable, especially when considering that spin-polarization is not included in either of the DFTB calculations. We note that the DFTB energies in our benchmark study are in much better agreement than reported elsewhere for radical species, which could be a consequence of a somehow biased test set in either evaluation study.[48] Either way, our benchmark clearly attests DFTB an accuracy on the order of the accuracy of B3LYP/6-311G** itself in the case of aromatic hydrocarbon radicals, with B3LYP only slightly more accurate by a few kcal/mol when compared to the *ab initio* G3-type level of theory. In light of the fact that the kinetic energy of a benzene molecule at 2500 K is around 50 kcal/mol, the DFTB accuracy (and in particular the comparatively excellent performance of the simple NCC-DFTB approach) in describing potential energy surfaces of hydrocarbon radical reactions seems to be sufficient. Nevertheless, to still further evaluate the performance of NCC- *versus* SCC-DFTB approaches for actual MD simulations of hydrocarbon radicals, we computed 10 trajectories based on the SCC-DFTB potential during a period of H abstraction and radical creation (details

are presented below in the discussion of the trajectories). As is explained in the Methods section, during DFTB/MD simulations we resorted to the use of electronic temperature T_e (for NCC-DFTB, $T_e = 5000$ K; for SCC-DFTB, $T_e = 2500$ K) in the electronic structure calculations during MD simulations. The electronic temperature allows fractional occupancies for molecular orbitals (MOs) and takes into account the near-degeneracy of quasi-degenerate singly occupied MOs (SOMOs) occurring in ensembles of radical species, which would otherwise lead to unphysical charge transfer in NCC-DFTB calculations. In SCC-DFTB, it also helps to accelerate SCC convergence of the wave function.[49] We find that DFTB/MD simulations employing SCC-DFTB during the period where hydrogen is present in the system essentially yield the same PAH growth rates and similar intermediate species of PAH growth as corresponding DFTB/MD simulations based only on NCC-DFTB simulations.

In summary, the benchmark studies described above justify the use of the computationally inexpensive NCC-DFTB level of theory in combination with appropriate electronic temperature for the quantum chemical potential underlying molecular dynamics simulations of benzene combustion at high temperatures. In the remainder of this article we will use the term "DFTB" in place of "NCC-DFTB" for simplicity.

Modeling Gas-Phase Benzene Oxidation. The starting model system for our nonequilibrium dynamics trajectories contained 36 benzene molecules (216 carbon and 216 hydrogen atoms) stacked in four layers of nine molecules arranged in a 3 × 3 quadratic plane in a cubic cell with an interlayer distance of 3.4 Å and closest intermolecular H-contacts of 2.2 Å (we denote this geometry as g1). Initial velocities were chosen randomly, adjusting the kinetic energy of the system to target temperatures. The total density was 0.50 g/cm^3, which is about half the density of liquid benzene (0.87 g/cm^3), and therefore arguably quite high. We have used such a high density to accelerate the initial PAH growth, but spontaneous density fluctuations are certainly possible in the real combustion systems. Unfortunately, there does not seem to be a systematic study on density fluctuations in combustion flames. Over the course of the simulations it became necessary to increase the cubic box side length from 21 Å to 30 Å for the pure carbon systems after 15.01 ps, as in several cases the graphitic cluster size approached the size of the PBC box. Therefore, the carbon density of the model system was initially 0.46 g/cm^3 during the first 15.01 ps of the trajectories, and 0.16 g/cm^3 afterward, which effectively mimics an expansion process and a density gradient. We further gradually lowered the H/C ratio during the simulations by removing 70 randomly selected hydrogen atoms from the system three times, at 5.00 ps, 10.02 ps, and 15.01 ps, reducing the total number of hydrogen atoms by 210 in the simulation system. Random numbers were generated by using the "Marsaglia uniform random number generator between 0.0 and 1.0 (using the public domain http://www.mathkb.com subroutine)". We also removed free hydrogen atoms when present at the time of random H removal. Free-hydrogen removal was performed before random-hydrogen removal. Hydrogen atoms were defined as "free" when they were separated from the nearest atom by a distance larger than a cutoff radius of 1.70 Å. In case of simulations where the nuclear temperature (T_n) was thermostatted at 3000 K, the removal of free hydrogens takes care of the remaining 6 hydrogens after 3 times 70 hydrogens are removed, while in simulations with $T_n = 2500$ K some of the six hydrogens stayed in the system and were finally taken out at the 20.02 ps mark. The benzene oxidation is therefore effectively simulated by removal of hydrogen instead of simulating explicit chemical reactions of O_2 molecules with the hydrocarbons, which would eventually lead to exothermic products H_2O, CO, and CO_2 *via* the more reactive radical species OOH and OH.

One may suspect that the simulation approach employed in this work is a crude oversimplification and results in an unrealistic acceleration of oxidation reactions, neglects defects created by CO_x elimination, and partially neglects the healing effects of annealing since our environmental temperatures are relatively high and the hydrogen removal steps follow each other very fast. Also, the experimentally observed important O_2 attack on phenyl leading to C_6H_5OO producing the cyclopentadienyl radical by way of CO_2 elimination cannot be included in MD simulations without actually including oxygen.[50] We are aware of these shortcomings. It is obvious that a fully realistic simulation would entail the consideration of (a) slower hydrogen removal rates, (b) much lower benzene densities, (c) O_2-induced oxidation reactions on the order of approximately 1 hydrogen atom/100 ps and (d) lower environmental temperatures on the order of $T_n < 2300$ K. All four "improvements" would lead to an increase in simulation time from several 100 ps to several 100 ns. Since it is impossible to perform such "realistic" simulations on present-day computers even with the relatively inexpensive DFTB potential, we settled for the currently possible type of simulation, while being aware that annealing processes as well as CO_x-created defects are severely underrepresented in this investigation. We therefore also refrain from detailed analysis regarding all possible reaction pathways occurring in our simulations and instead focus more on the qualitative aspects of cluster growth such as fragment size, H/C ratio, carbon sp^2- *versus* sp-hybridization, and ring count statistics as functions of simulation time. We also take comfort in the fact that important aromatic−aliphatic linked species such as reactions with acetylene[9,10,40] (the HACA route) are naturally included and well-described in the present simulation approach. The details of the 80 NCC-DFTB

TABLE 2. List of Successful Simulations with T_n = 2500 K[a]

	H's removed (free/random)						
trajectory name	@5.00 ps	@10.02 ps	@15.01 ps	t_f (ps)	#C_{cage}	#$C_{cluster}$	curvature (1/Å)
B2500Kg1_4	1/70	1/70	1/70	70.23	178	198	0.141
B2500Kg1_5	1/70	0/70	0/70	44.33	184	184	0.125
B2500Kg1_7	1/70	0/70	0/70	67.21	193	195	0.131
B2500Kg1_8	1/70	0/70	0/70	45.06	177	195	0.151
B2500Kg1_11	1/70	1/70	0/70	57.29	192	200	0.147
B2500Kg1_12	1/70	1/70	0/70	121.77	212	212	0.133
B2500Kg1_14	1/70	0/70	0/70	43.05	202	202	0.131
B2500Kg1_16	1/70	1/70	0/70	165.31	203	208	0.125
B2500Kg1_18	1/70	1/70	0/70	153.44	204	208	0.145
B2500Kg1_19	1/70	0/70	0/70	55.05	174	189	0.132

[a] t_f corresponds to time of closed cage formation; #C_{cage} is the number of carbon atoms in the cage only, and #$C_{cluster}$ is the number of total carbon atoms in the cluster at the time of cage formation. Curvature corresponds to root mean square (rms) curvature of the cluster (#$C_{cluster}$). The rms curvature is defined as the average of inverse radii of spheres best fitted to a sp^2-carbon atom plus its three bond neighbors.

trajectories and 10 SCC-DFTB benchmark trajectories are given in Tables 2−7, grouped by nuclear temperature T_n and whether a fullerene cage was formed ("successful") or not ("unsuccessful") during the maximum simulation time of 225.21 ps.

Description of Trajectories. We computed two sets of DFTB/MD trajectories: 20 low-temperature trajectories with T_n = 2500 K (Tables 2 and 3), and 60 high-temperature trajectories with T_n = 3000 K (Tables 4 and 5). In the case of T_n = 2500 K, the same initial Cartesian coordinates (denoted g1, see section "Modeling Gas-Phase Benzene Oxidation") were used as starting points for all trajectories, and different trajectories were generated only by changing the random number sequence for randomly removing hydrogen atoms. We identify the trajectories by their names as B2500Kg1_*n*, where "B2500K" stands for 36 benzenes simulated at T_n = 2500 K, "g1" stands for the choice of the initial Cartesian coordinates, and "_*n*" is a running number *n* = 1−20 for the 20 trajectories. In the case of T_n = 3000 K, four different initial geometries (denoted by g1, g2, g3, and g4) were considered as starting structures for 20, 15, 15, and 10 trajectories in each case, respectively. The g*x* (*x* = 1−4) coordinates were generated by changing the interlayer distances between benzene layers by 0.2 Å (g2, one outer layer of g1 is moved inward by 0.2 Å; g3, one outer layer of g1 is moved outward by 0.2 Å; g4, two outer layers of g1 are moved inward by 0.2 Å). Since positions of benzene molecules randomize rapidly because of high temperature, the exact initial positions of individual benzene molecules do not matter.

Ten benchmark simulations for T_n = 2500 K using SCC-DFTB with T_e = 2500 K during hydrogen removal until *t* = 15.01 ps, followed by NCC-DFTB with T_e = 2500 K for the practically pure carbon system, are named BSN2500Kg1_1 to BSN2500Kg1_10, and the 4 successful cases from these simulations are listed in Table 6. In all cases we recorded the number of removed hydrogen atoms after 5.00, 10.02, and 15.01 ps, separated by free hydrogen and random hydrogen removal. In the case of successful cage formation (Tables 2, 4, and 6), we recorded the time of (closed) cage formation t_f, the number of carbon atoms in the cage C_{cage} at time t_f, the total number of carbon atoms in the largest cluster $C_{cluster}$, and the root-mean-square (rms) curvature for the resulting giant fullerene. (The rms curvature is defined as the average of inverse radii of spheres best fitted to a sp^2-carbon atom plus its three bond neighbors.) The difference between #C_{cage} and #$C_{cluster}$ includes the number of "antenna" carbon atoms, carbon atoms attached outside of the cage usually as polyyne chains. Self-assembled giant fullerene cages in

TABLE 3. List of Unsuccessful Simulations with T_n = 2500 K[a]

	H's removed (free/random)				
trajectory name	@5.00 ps	@10.02 ps	@15.01 ps	*t* (ps)	#$C_{cluster}$
B2500Kg1_1	1/70	0/70	0/70	29.35	202
B2500Kg1_2	1/70	0/70	0/70	225.21	200 (defective cage)
B2500Kg1_3	1/70	1/70	2/70	28.96	202
B2500Kg1_6	1/70	3/70	0/70	29.47	206
B2500Kg1_9	1/70	0/70	0/70	113.75	206 (one end open cage)
B2500Kg1_13	1/70	0/70	0/70	200.27	212 (defective cage)
B2500Kg1_15	1/70	0/70	0/70	35.79	203
B2500Kg1_17	1/70	0/70	0/70	33.12	216
B2500Kg1_20	1/70	1/70	0/70	63.54	214

[a] *t* corresponds to time when the simulation was terminated; #$C_{cluster}$ is the number of carbon atoms in the largest cluster formed at time *t*.

TABLE 4. Successful Simulations with T_n = 3000 K[a]

	H's removed (free/random)						
trajectory name	@5.00 ps	@10.02 ps	@15.01 ps	t_f (ps)	#C_{cage}	#$C_{cluster}$	curvature (1/Å)
B3000Kg1_1	4/70	2/70	0/70	28.81	120	165	0.145
B3000Kg1_2	4/70	0/70	0/70	50.34	149	152	0.152
B3000Kg1_3	4/70	1/70	2/69	56.96	135	180	0.159
B3000Kg1_4	4/70	2/70	0/70	63.82	190	192	0.137
B3000Kg1_13	4/70	1/70	1/70	37.99	191	193	0.141
B3000Kg1_15	4/70	3/70	2/67	32.54	169	179	0.142
B3000Kg2_2	3/70	0/70	0/70	49.46	185	191	0.132
B3000Kg2_3	3/70	0/70	0/70	59.45	179	198	0.135
B3000Kg2_5	3/70	0/70	0/70	49.83	179	179	0.142
B3000Kg2_6	3/70	0/70	0/70	39.52	174	180	0.140
B3000Kg2_7	3/70	2/70	1/70	35.22	160	184	0.150
B3000Kg2_10	3/70	0/70	1/70	51.76	183	183	0.142
B3000Kg2_12	3/70	0/70	1/70	54.61	188	200	0.138
B3000Kg2_13	3/70	1/70	2/70	49.99	185	185	0.136
B3000Kg3_3	6/70	1/70	2/67	77.46	201	202	0.141
B3000Kg3_4	6/70	1/70	0/69	55.53	157	166	0.138
B3000Kg3_7	6/70	1/70	0/69	22.39	74	168	0.168
B3000Kg3_8	6/70	1/70	1/68	39.14	188	198	0.130
B3000Kg3_13	6/70	1/70	0/69	26.88	80	203	0.163
B3000Kg3_14	6/70	2/70	0/68	37.36	190	190	0.129
B3000Kg4_3	6/70	2/70	2/66	37.74	167	180	0.145
B3000Kg4_6	6/70	0/70	1/69	31.41	88	190	0.167
B3000Kg4_7	6/70	0/70	2/68	46.73	176	177	0.129
B3000Kg4_9	6/70	2/70	0/68	81.99	199	201	0.117
B3000Kg4_10	6/70	1/70	0/69	42.17	111	200	0.152

[a] t_f corresponds to time of closed-cage formation; #C_{cage} is the number of carbon atoms in the cage only, and #$C_{cluster}$ is the number of total carbon atoms in the cluster at the time of cage formation. Curvature corresponds to rms curvature (Table 2) of the cluster (#$C_{cluster}$).

a carbon-rich environment possess at the earliest stages polyyne chains still attached to sp^3-hybridized carbon atoms,[12,13,15] which quickly fall off as a consequence of the π-stabilization energy gain after removal of these defects. Here, however, this difference can also become indicative of graphene sheets or large clusters still attached to the closed fullerene cage. In the case of unsuccessful cage formation (Tables 3, 5, and 7), we record the size of the largest carbon cluster, and the time at which the trajectory was terminated. In the case of successful cage formations, the simulation was stopped soon after the cage closure.

Self-Assembled Giant Fullerenes. Among the B2500Kg1_*n* low-temperature set of trajectories, 10 were found to form a closed giant fullerene cage with a size range from C_{174} to C_{212}, listed in Table 2. The success rate in this case is 10/20 = 50% (our fullerene "yield"). Among the B3000Kg*n* high-temperature set of trajectories, 25 formed closed giant fullerene cages within or around 70 ps of time with a size range from C_{74} to C_{200}, shown in Table 4. The success rate (or yield) in this case is therefore slightly lower with 25/60 = 42%, but such a small difference is beyond the rather low statistical significance of the few trajectories performed here. Similar to our previous pure carbon size-up simulations, we do not find that C_{60} forms directly, but rather that GFs appear, *notably only after all hydrogen atoms have been removed from the system*, with cage member numbers on the order of the number of carbon atoms present in the simulation. The overall fullerene yield in the present simulations is noticeably higher than our previous results; fullerene self-assembly from pure C_2 molecules only produced 8 out of 35 total simulations (yield: 23%) under the best conditions.[14]

The average cage sizes and corresponding rms curvatures of the giant fullerenes at T_n = 2500 K are 191.9 and 0.136 $Å^{-1}$, and at T_n = 3000 K they are 160.7 and 0.143 $Å^{-1}$. The smallest and largest cages produced at T_n = 2500 K are 174 and 212 (just 4 smaller than the maximum 216), while at T_n = 3000 K they are 74 and 201. Clearly, the higher temperature simulations tend to produce smaller fullerene cages. The average time of cage formation $\langle t_f \rangle$ is similarly dependent on the temperature; at T_n = 2500 K, $\langle t_f \rangle$ = 82.3 ps, while it is nearly half for T_n = 3000 K with $\langle t_f \rangle$ = 46.4 ps. We will discuss these significant findings later when analyzing the cluster size distribution as a function of time.

As in our previous simulations of pure carbon systems, the average rms curvatures of self-assembled GFs are higher than one would expect for spherical cages, but much lower than the curvature required for $^{Ih}C_{60}$, which has an rms curvature of 0.28 $Å^{-1}$. If the cages were spherical, a 0.13 $Å^{-1}$ rms curvature would correspond to a radius of 7.69 Å and therefore contain more than 240 atoms (the radius of $^{Ih}C_{240}$ is ~7.3 Å). Generally, the cages emerge with very nonspherical

TABLE 5. Unsuccessful Simulations with T_n = 3000 K[a]

	H's removed (free/random)				
trajectory name	@5.00 ps	@10.02 ps	@15.01 ps	t (ps)	# $C_{cluster}$
B3000Kg1_5	4/70	2/70	1/69	25.89	179
B3000Kg1_6	4/70	0/70	1/70	24.24	208
B3000Kg1_7	4/70	0/70	0/70	40.24	199
B3000Kg1_8	4/70	1/70	2/69	33.77	202
B3000Kg1_9	4/70	0/70	1/70	42.51	204
B3000Kg1_10	4/70	2/70	1/69	43.10	185
B3000Kg1_11	4/70	0/70	1/70	30.30	192
B3000Kg1_12	4/70	2/70	0/70	52.76	206
B3000Kg1_14	4/70	1/70	0/70	46.58	196
B3000Kg1_16	4/70	2/70	1/69	35.97	208
B3000Kg1_17	4/70	2/70	0/70	70.06	198
B3000Kg1_18	4/70	2/70	1/69	29.19	189
B3000Kg1_19	4/70	1/70	1/70	30.93	177
B3000Kg1_20	4/70	0/70	2/70	33.38	189
B3000Kg2_1	3/70	0/70	0/70	35.15	196
B3000Kg2_4	3/70	0/70	2/70	32.11	190
B3000Kg2_8	3/70	2/70	0/70	45.15	200
B3000Kg2_9	3/70	0/70	1/70	31.90	197
B3000Kg2_11	3/70	2/70	0/70	32.99	195
B3000Kg2_14	3/70	2/70	1/70	30.03	183
B3000Kg2_15	3/70	1/70	0/70	37.06	181
B3000Kg3_1	6/70	0/70	0/70	24.00	180
B3000Kg3_2	6/70	2/70	1/70	34.04	199
B3000Kg3_5	6/70	0/70	2/70	26.34	185
B3000Kg3_6	6/70	0/70	2/70	40.84	190
B3000Kg3_9	6/70	1/70	1/70	33.59	185
B3000Kg3_10	6/70	0/70	1/70	25.02	201
B3000Kg3_11	6/70	2/70	1/70	26.14	198
B3000Kg3_12	6/70	2/70	0/70	21.73	192
B3000Kg3_15	6/70	0/70	0/70	32.11	200
B3000Kg4_1	6/70	3/70	0/70	34.53	208
B3000Kg4_2	6/70	0/70	1/70	39.66	190
B3000Kg4_4	6/70	0/70	0/70	180.16	defective cage, 204
B3000Kg4_5	6/70	0/70	1/70	185.17	defective cage, 202
B3000Kg4_8	6/70	0/70	0/70	28.72	191

[a] t corresponds to time when the simulation was terminated; #$C_{cluster}$ is the number of carbon atoms in the largest cluster formed at time t.

shape and therefore larger local curvature values are observed.

A noticeable difference to our previous simulation is the fact that the number of carbon atoms in the polyyne "antennas" is small, sometimes even zero, which means that the cages were closed without attached polyyne chains. The average for #$C_{cluster}$−#C_{cage} and the number of trajectories where this difference is zero are at T_n = 2500 K 7.2 and 3, and at T_n = 3000 K 24.7 and also 3. The number of exo (outside)-cage carbon atoms in the cluster sometimes includes attached graphene sheets as well in these simulations, in particular this occurs in high-temperature simulations. For instance in the case of B3000Kg3_7 the fullerene cage itself has only 74 carbon atoms but the recorded cluster is larger by 94 carbon atoms at the time of cage self-assembly. In our previous C_2-feedstock simulations we never encountered such attached graphene sheets, and

TABLE 6. List of Successful Simulations Using SCC-DFTB (Followed by NCC-DFTB) with T_n = 2500 K, T_e = 2500 K[a]

	H's removed (free/random)						
trajectory name	@5.00 ps	@10.02 ps	@15.01 ps	t_f (ps)	#C_{cage}	#$C_{cluster}$	curvature (1/Å)
BSN2500Kg1_1	0/70	0/70	7/69	60.59	186	208	0.135
BSN2500Kg1_2	0/70	0/70	3/70	80.07	202	204	0.145
BSN2500Kg1_6	0/70	0/70	5/70	197.88	202	204	0.131
BSN2500Kg1_7	0/70	0/70	0/70	155.11	200	200	0.140

[a] t_f corresponds to time of closed cage formation; #C_{cage} is the number of carbon atoms in the cage only, and #$C_{cluster}$ is the number of total carbon atoms in the cluster at the time of cage formation. Curvature corresponds to rms curvature (Table 2) of the cluster (#$C_{cluster}$).

TABLE 7. List of Unsuccessful Simulations Using SCC-DFTB (Followed by NCC-DFTB) with T_n = 2500 K, T_e = 2500 K[a]

	H's removed (free/random)				
trajectory name	@5.00 ps	@10.02 ps	@15.01 ps	t (ps)	#$C_{cluster}$
BSN2500Kg1_3	0/70	0/70	5/70	100.9	214
BSN2500Kg1_4	0/70	0/70	0/70	80.07	202
BSN2500Kg1_5	0/70	0/70	6/70	60.05	197
BSN2500Kg1_8	0/70	0/70	0/70	75.05	211
BSN2500Kg1_9	0/70	0/70	6/70	214.89	210
BSN2500Kg1_10	0/70	0/70	0/70	70.06	206

[a] t_f corresponds to time when the simulation was terminated; #$C_{cluster}$ is the number of carbon atoms in the largest cluster formed at time t.

we attribute the present finding to noticeable differences in the fullerene growth mechanism between pure carbon and hydrocarbon combustion synthesis. We will discuss this result also later in greater detail.

Key Events During Self-Assembly of Giant Fullerenes. In the following sections, we will analyze in greater detail the sequence of events for successful trajectories of both low- and high-temperature simulations and will illustrate key points using one trajectory from each T_n as a representative case, namely B2500Kg1_19 and B3000Kg1_1. Plots of the relative potential energies of two trajectories B2500Kg1_19 and B3000Kg1_1 during the full lengths of the trajectories are shown in Figure 1, where "jumps" correspond to the hydrogen removal. Successful trajectories at the same temperatures followed qualitatively similar pathways as these two cases, with the most important variations in the time required for cage formation t_f. Unsuccessful trajectories are characterized by structures that have smaller uniform curvature and appear more sheet-like at the end of the simulations. Detailed information such as cluster growth, hybridization statistics, and ring formation statistics for selected additional successful and unsuccessful trajectories are given in the Supporting Information.

Initial Reactions, PAH Formation, and C/H Ratio: The First 5 ps. We originally intended to equilibrate the systems at constant temperature for 5.00 ps before the first H removal step. However, during this time span various radical reactions were observed due to thermal decompositions and high benzene density, particularly at high temperature. Since no hydrogen atoms were removed, trajectories with different n in B2500Kg1_n and B3000Kgx_n are identical at this stage. It is apparent from Figure 1 that at higher temperature the system climbs up the potential energy (PE) landscape faster than during low-temperature simulations, with a rate of about 3000 kcal/mol/5 ps for T_n = 3000 K as opposed to about 2000 kcal/mol/5 ps for T_n = 2500 K. The hydrocarbon species different from benzene, resulting from reactions occurring at T_n = 2500 K, were products of hydrogen abstractions 5C_6H_5, 2C_6H_7, H_2, and H; clearly the carbon framework of the benzene molecules remained intact at this stage. On the other hand, the nonbenzene species created at T_n = 3000 K were more complex and included modifications of the carbon frameworks: $C_{12}H_9$, C_8H_8, C_8H_5, 2C_6H_8, 3C_6H_7, 2C_6H_5, 2C_6H_4, 2C_2H_2, C_2H, C_2, $2H_2$, 4H for all trajectories starting with geometry g1; $C_{21}H_{18}$, $C_{12}H_6$, C_9H_9, C_7H_7, C_7H_6, 2C_6H_8, 4C_6H_7, 2C_6H_5, 2C_2H_2, 3C_2H, 2C_2, CH_4, CH_2, $2H_2$, 3H for those starting with g2; $C_{12}H_{12}$, $C_{12}H_{10}$, 2$C_{12}H_9$, C_9H_9, 2C_6H_7, 3C_6H_5, C_6H_4, C_4H_7, C_4H_6, C_4H_4, C_3H_5, C_2H_2, 3C_2H, H_2, 6H for g3; and 2$C_{12}H_{10}$, $C_{12}H_9$, C_6H_8, 6C_6H_7, 8C_6H_5, C_4H_4, C_2H, H_2, 6H for g4. Trajectory snapshots of these structures are shown in Figure S6 of the Supporting Information. Several structures among these species such as methyl (here as CH_4),[51] ethynyl (C_2H),[52] acetylene (C_2H_2),[51,53] C_3H_5,[52] C_4H_7,[52] phenyl (C_6H_5),[52,53] C_7H_7,[52] phenylacetylene (C_8H_6),[53] and biphenyl ($C_{12}H_{10}$)[37] have been indentified in benzene/oxygen/argon flames. $C_{12}H_{10}$, C_8H_8, C_7H_6, C_6H_8, C_6H_4, C_6H_5, C_4H_6, C_4H_4, and H_2 were identified also in another benzene/oxygen/argon experiment.[54] Under these circumstances, the initial 5 ps should not be regarded as an equilibration period, but represent initiation reactions preceding any programmed hydrogen removal. They are typically hydrogen abstractions, creating at first phenyl and H atom radical species: $C_6H_6 \rightarrow C_6H_5 + H$. Follow-up reactions of this abstraction as listed in Table 8 become generally much faster once the phenyl and H radical species are created. In particular, the radical H is sometimes found to react with abun-

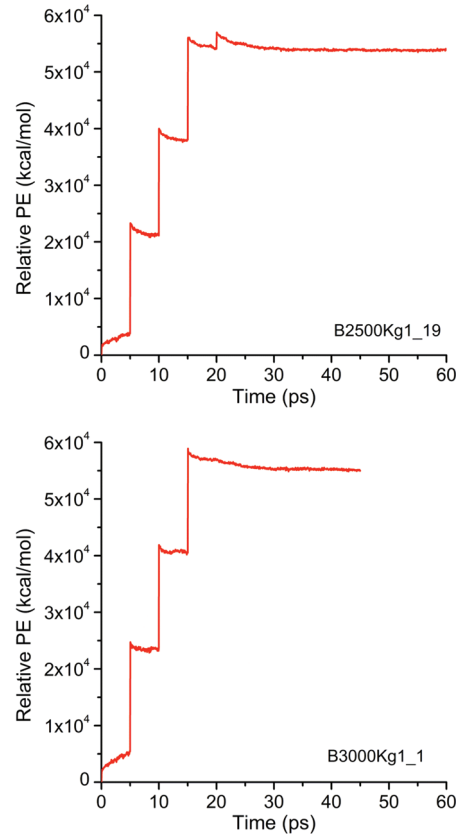

Figure 1. Change in relative potential energy (PE) during the course of the B2500Kg1_19 (top) and B3000Kg1_1 (bottom) trajectories, with initial PE of the starting geometry as reference. Jumps in energy correspond to the hydrogen removal.

TABLE 8. Initiation Reactions and Species Created during the First 5.00 ps with H/C = 1

T_n = 2500K (B2500Kg1_n)	T_n = 3000K, (B3000Kg1_n)
$C_6H_6 \rightarrow C_6H_5 + H$ (1.94, 2.60, 2.84, 3.01 ps)	$C_6H_6 \rightarrow C_6H_5 + H$ (1.65, 1.73, 1.74, 1.96,... ps)
$C_6H_6 + H \rightarrow C_6H_7$ (2.05, 3.03, 3.97 ps)	$C_6H_6 + H \rightarrow C_6H_7$ (1.77, 1.98,... ps)
$C_6H_7 + H \rightarrow C_6H_8 \rightarrow C_6H_6 + H_2$ (4.01 ps)	$C_6H_5 \rightarrow C_6H_4 + H$ (1.88, 2.49 ps)
	$C_6H_6 + C_6H_4 \rightarrow C_{12}H_{10} \rightarrow 2C_6H_5$ (2.25 ps)
	$C_6H_6 + C_4H_4 \rightarrow C_{10}H_{10}$ (2.61 ps)
	$C_{10}H_{10} \rightarrow C_8H_7 + C_2H_3$ (2.83 ps)
	$C_2H_3 \rightarrow C_2H + H_2$ (3.66 ps)
	$C_6H_6 + C_2H \rightarrow C_6H_7 + C_2$ (3.81 ps)

dant benzene to create the C_6H_7 radical, which can be regarded as an artifact of our oxygen-free high-temperature simulations. At T_n = 3000 K, further decomposition reactions such as $C_6H_5 \rightarrow C_6H_4 + H$, C_6H_6 (benzene) $\rightarrow C_6H_5$ (phenyl radical) $\rightarrow C_6H_4$ (*ortho*-benzyne) $\rightarrow C_6H_3(H_2)$ (1-yne 2, 3-diene cyclohexane) $\rightarrow C_6H_6$ (1,4,6-cyclohexatriene or *meta*-C_6H_6) $\rightarrow$ acyclic-C_6H_6 (ring-opening) $\rightarrow C_4H_4$ (vinylacetylene) + C_2H_2 (acetylene) and $C_2H_3 \rightarrow C_2H + H_2$ are observed. In some cases, species containing five-membered rings are also observed during this initial reaction period (e.g., C_7H_7, C_7H_6 for g2 and $C_{12}H_{12}$, C_9H_9 for g3). The collision rates and occurrence of bimolecular reactions are high since the simulations were performed under high pressure conditions. From a statistics of bimolecular collisions/reactions occurring during the first 15 ps of simulations (Figure S7) we observed that, as expected, at higher temperature (3000 K) the number of reactions/collisions is much higher than at lower temperature (2500 K). Also, the number of reactions is much higher during the time interval 5 to 10 ps, because during this time interval several radical species are present (H/C ratio $\approx$ 0.66). During 0−5 and 10−15 ps time intervals the number of radical species are lower either because of higher H/C ratio (for 0−5 ps) or due to formation of larger clusters and healing of radical defects (10−15 ps). We also noted that the number of reactions involving the radical C_2H species is higher than with the closed-shell C_2H_2 species. For lower H/C ratios ($\sim$0.66 and $\sim$0.33), a significant number of collision/reactions is observed with C_2 species. As expected, during the time interval 5−10 ps (with H/C ratio $\sim$0.66) the collisions/reactions of radical species like C_6H_5, C_6H_4, C_6H_3 are significant. The species C_6H_5 and C_6H_4 show almost equal collisions/reactions probability because of their almost equal abundance. In experimental conditions it is expected that the species C_6H_5 and C_6H_4 are likely to take part in the growth processes.

Analysis of Intermediate Species as Function of H/C Ratio. To illustrate quantitatively the events occurring in successful trajectories for the two temperatures, we chose the same two representative trajectories B2500Kg1_19 and B3000Kg1_1 to plot the quantities of interest. In Figure 2 we display histograms for the number of carbon atoms in the C/H and C fragments. In Figure 3, we give histograms for the number of mono- or divalent (sp-), trivalent (sp^2-) and tetravalent (sp^3-) type carbons (#sp^n-type). Their numbers were derived from the number of bond partners (C as well as H) in snapshot geometries and do therefore not necessarily reflect the actual electronic hybridization state of the carbon atoms. At time t = 0.00 ps, all 216 atoms are of trivalent sp^2-type (36 benzene molecules). Since the number of sp^3-type carbons is always almost negligible under the conditions of the simulations, the plots record mainly the interconversion between sp^2- and sp-type carbons, and the corresponding curves are therefore symmetric around 108 (half the number of carbon atoms, as #sp^2 = $\sim$216 − #sp and *vice versa*). In Figure 4 the number of three-

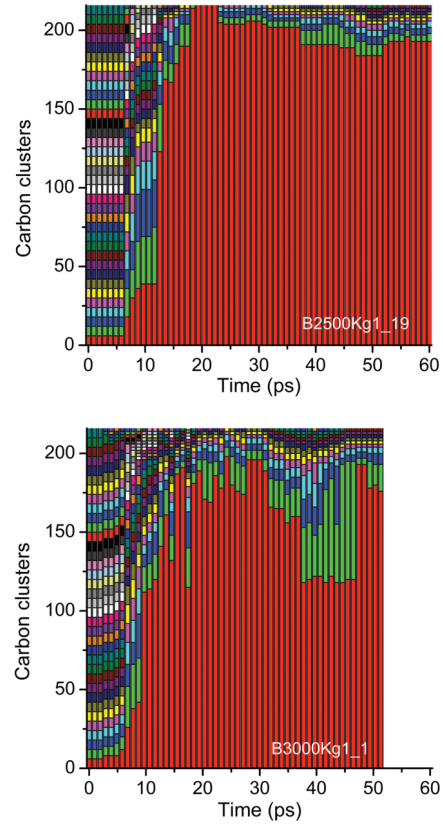

Figure 2. Count of the number of carbon atoms in clusters as a function of time for B2500Kg1_19 (top) and B3000Kg1_1 (bottom) trajectories. There are 216 total carbon atoms, and the number of carbon atoms belonging to separate molecular structures in the reaction system are shown at time intervals of 1 ps as vertical bars, beginning from 36 benzene molecules, with one cluster gradually consuming smaller fragments (shown in red).

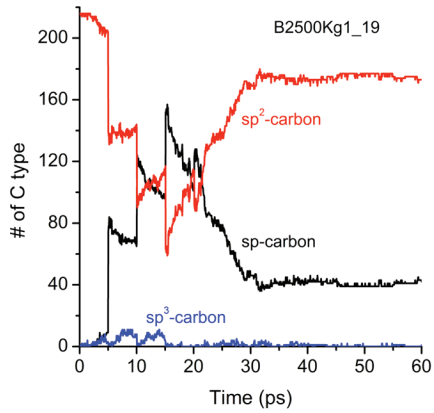

Figure 3. Carbon hybridization count [(black) sp-, (red) sp^2- and (blue) sp^3-type carbons] as a function of time for B2500Kg1_19 (top) and B3000Kg1_1 (bottom) trajectories.

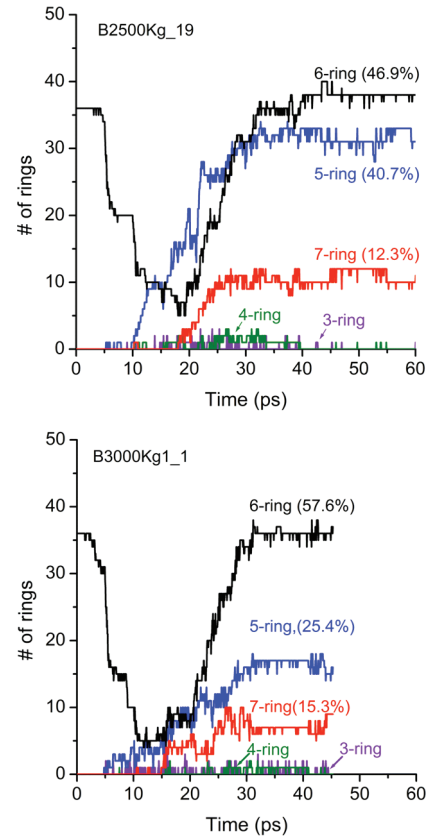

Figure 4. Ring count statistics as a function of time for B2500Kg1_19 (top) and B3000Kg1_1 (bottom) trajectories. Three−seven-membered rings are considered in the count.

to-seven-membered rings are plotted as a function of simulation time for the two trajectories. Plots of the same type for additional trajectories for selected successful and unsuccessful cases are given in the Supporting Information. As these data are interdependent, we discuss all of them together in the subsequent paragraphs.

First H Removal. A total of 70 randomly chosen H atoms and any free H atoms present in the system were removed at $t = 5.00$ ps for the first time; 70 radical species were created at once, where ~26% of molecular units are unaffected, ~40% are affected by single-H abstractions, ~25% experience dual-H abstractions, and the rest suffer three- and higher number H abstractions. This distribution corresponds roughly to the statistical distribution one would expect as a result of random hydrogen removal from an infinitely large sample of benzene molecules. Obviously, double H abstractions on the same benzene molecules produces *ortho*-benzyne (C_6H_4) and phenylene biradicals (C_6H_4) such as *para*-benzyne and *meta*-benzyne species. We observed that among these radical species, *para*-benzyne units are particularly unstable, and undergo ring-opening. The resulting linear polyacetylene-like chains were then observed to add themselves onto aromatic rings, or are sometimes broken into smaller fragments during this process. On the other hand, *ortho*-benzyne species are comparatively stable and they form biphenylene like structures. They also are found to react with other species or H-radical to form C_6H_5 ($C_6H_4 + H \rightarrow C_6H_5$) and finally C_6H_6 ($C_6H_5 + H \rightarrow C_6H_6$). The *meta*-benzyne radical species may form *para*-benzyne due to unimolecular H-migration, then following the same fate as the directly created *para*-benzynes. We observed that among tridehydrobenzene radicals, 1,2,4-tridehydrobenzenes are very unstable and undergo ring-opening easily. In some cases, 1,2,4-tridehydrobenzene (C_6H_3) reacted with a H-radical ($C_6H_3 + H \rightarrow C_6H_4$) forming *para*-benzyne (C_6H_4), followed by ring-opening. On the other hand, 1,2,3-tridehydrobenzene (C_6H_3) and 1,3,5-tridehydrobenzene are (C_6H_3) less likely to undergo ring-opening, and these radical species react preferentially with other species to form biphenyl-like structures before undergoing further reactions. The number of C_6H_2-like radical species created was only on the order of 1%, and these species undergo ring-opening very fast. We never observed C_6H or C_6 during our H abstraction, inline with the statistical expectation that the formation of these species is extremely unlikely during random H elimination.

As a consequence of the H removal, the number of trivalent carbon atoms (#sp^2-type) was suddenly reduced by 70, and the number of divalent carbon atoms #sp-type increased correspondingly (see Figure 3).

However, the number of sp^2-species has a tendency to recover after 5 ps for the $T_n = 2500$ K regime, when subsequent reactions increase the number of trivalent carbon atoms. In contrast, at $T_n = 3000$ K the divalent carbon atoms are prevented by the higher temperature from saturating their free valences, and the number of sp^2-species even reduces after 5 ps. Similar characteristics for sp- and sp^2-species at both temperatures are also obtained at the times of the second ($t = 10.02$ ps) and third H ($t = 15.01$ ps) removal.

Figure 4 illustrates a continued decrease in the number of six-membered rings at both temperatures, with little to no formation of five- or seven-membered ring species. Figure 2 demonstrates that at $T_n = 2500$ K, during the period following the first H removal, C_6H_x-C_6H_y dimerizations take place but very little growth of larger clusters occurs, while during the same period at $T_n = 3000$ K, significant growth of a branched polyacetylene-like structure sets in. Accompanying these processes was a sudden rise in total energy as well as in the potential energy of the system. During the course of the next 5 ps, the PE continued to decrease. In summary, we found that a C/H ratio of ~0.66 at the temperatures under consideration promotes ring-opening and polyacetylene-like chain formation rather than PAH growth.

Second H Removal. Next, hydrogen atoms were removed from the system at $t = 10.02$ ps for the second time leaving the system now with only about one-third of the initial number of hydrogen atoms (H/C ratio close to 0.3). Immediately following the second H removal we found that the number of six-membered rings reached a minimum in the simulations (see Figure 4). For $T_n = 3000$ K only about 10% of the original number of C_6 units remained intact as a cyclic species, while for $T_n = 2500$ K the number of surviving six-membered rings was higher, about 30%. At the same time, for $T_n = 3000$ K, the largest cluster has reached its maximum size, while for $T_n = 2500$ K we find that the largest cluster continues to grow until the end of the second H removal period, up to 15 ps (see Figure 2). In both cases, as a consequence of the dramatic increase in polyacetylene-like hydrogen-deficient carbon chains (Figure 3), spontaneous ring formation and thus PAH growth set shortly after 10 ps (Figure 4). Accompanying these processes was a rapid decrease in PE due to C−C PAH network formation and increasing π-conjugation (see Figure 1). In summary, we found that the H/C ratio of ~0.66 promotes PAH growth; however, owing to the rather chaotic condensation processes following the preceding violent ring-opening period for H/C = ~0.33, a significant number of five- and also seven-membered rings became incorporated into the growing PAH's.

Third H Removal. We finally performed the H removal for the third time at $t = 15.01$ ps, after which (in almost all cases) all hydrogen atoms were removed from the system. At this time, a large PAH cluster had already formed (Figure 2), containing several five-, six-, and some seven-membered rings, and the sudden H removal initiated a massive ring formation process in the existing cluster rather than further polyacetylene-like cluster growth (Figure 4). Figure 3 illustrates clearly that a maximum in the number of sp-hybridized carbon atoms is reached at $t = 15.01$ ps, from which point onward their numbers systematically decrease because of the increase in sp^2-hybridized carbon atoms. The sp/sp^2 ratio seems to reach an equilibrium value that depends less on the temperature but rather on the configuration of the largest cluster. Closed cages are finally formed at $t_f = 55.05$ ps (for B2500Kg1_19) and $t_f = 28.81$ ps (for B3000Kg1_1).

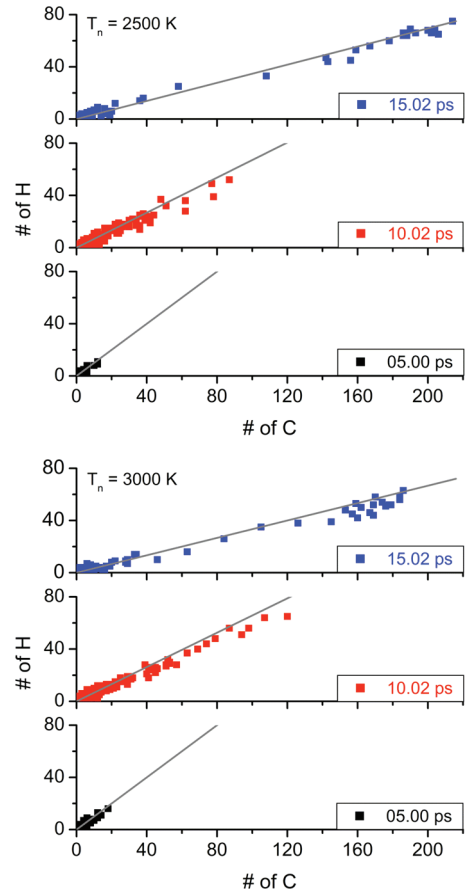

Figure 5. Hydrocarbon size and composition at 5.00, 10.02, and 15.02 ps (just before the H removal step). Each point corresponds to a species of the form C_xH_y. The continuous gray line corresponds to the H/C ratio of the ensemble at that time. The upper data corresponds to 2500 K, the lower data corresponds to 3000 K simulation temperature (data points are plotted for all B2500Kg1_*n* and B3000Kg1_*n* with *n* = 20 trajectories).

The H/C composition of hydrocarbons during the first 15 ps as a function of time is displayed in Figure 5. Data points are plotted for all 20 g1 trajectories for both simulations temperatures $T_n = 2500$ and $T_n = 3000$ K. Each data point on the graph corresponds to a hydrocarbon of the form C_xH_y. To determine stoichiometry of hydrocarbon species encountered in the trajec-

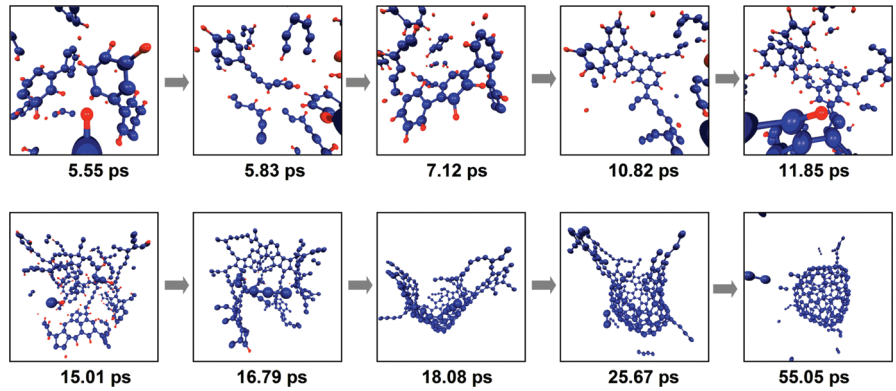

Figure 6. Snapshots from B2500Kg1_19 showing key events. Positions of the carbon and hydrogen atoms are represented by big (blue) and small (red) spheres, respectively.

tories (in other words, the H/C ratio), we used cutoff radii of 1.90, 1.70, and 1.50 Å for C−C, C−H, and H−H bond length, respectively. These cutoff radii are the result of extensive numerical tests regarding the stability of the counting in the present hot (vibrationally excited) systems. The straight line corresponds to the overall H/C ratio of the system: H/C = 1 up to t = 5.00 ps, H/C ≈ 0.66 during t = 5.00−10.02 ps and H/C ≈ 0.33 during t = 10.02−15.02 ps. This figure shows that for T_n = 3000 K and H/C ≈ 0.66, the cluster sizes become larger more rapidly and the system is therefore obviously more reactive than in the case of T_n = 2500 K. After 10.02 ps of simulations the largest cluster consists of ~80 carbon atoms for T_n = 2500 K whereas we find a size of ~120 for T_n = 3000 K. The clusters in this case are open-chain polyacetylene-like structures. After 15.02 ps we find that the largest clusters are present at the *lower* temperature (2500 K), just before final H removal, but with larger clusters more widely distributed in size compared to T_n = 3000 K, where the cluster size seems highly concentrated around 170 carbon atoms. The clusters in this case are condensed PAHs and giant fullerene precursors. As an overall trend we note that larger clusters tend to have only slightly lower H/C ratios than the average value, while smaller fragments have correspondingly slightly higher H/C ratios. Most importantly, as long as hydrogen is present in the system, *we do not find a preference in growth toward maximally conjugated PAHs* with significantly lower H/C ratios than the system's H/C ratio.

DISCUSSION

The Mechanism of Giant Fullerene Cage Formation. To highlight the differences between the fullerene cage formation as a consequence of benzene combustion on one hand and aggregation of C_2 molecules on the other, it is helpful to recall briefly the three stages of giant fullerene cage self-assembly in systems with continuous C_2 supply:[11,13,14] (1) *nucleation* of polycyclic structures from entangled polyyne sp-carbon chains, (2) cluster *growth* by ring condensation of carbon chains and macrocycles attached to the hexagon and pentagon containing nucleus, and (3) *cage closure*. In benzene combustion simulations we are dealing with apparently two rather different episodes with qualitatively different behavior regarding chemical reactivity. For H/C ratio higher than ~0.66, rings are broken/open and radical defects are created as a function of H abstraction and subsequent radical reactions. Figure 6 (5.55 and 7.12 ps for B2500Kg1_19) and Figure 7 (3.20 ps, for B3000Kg1_1) are showing such exemplary ring fragmentation reactions for the two simulation temperatures, and polyacetylene-like chains attached to five-,

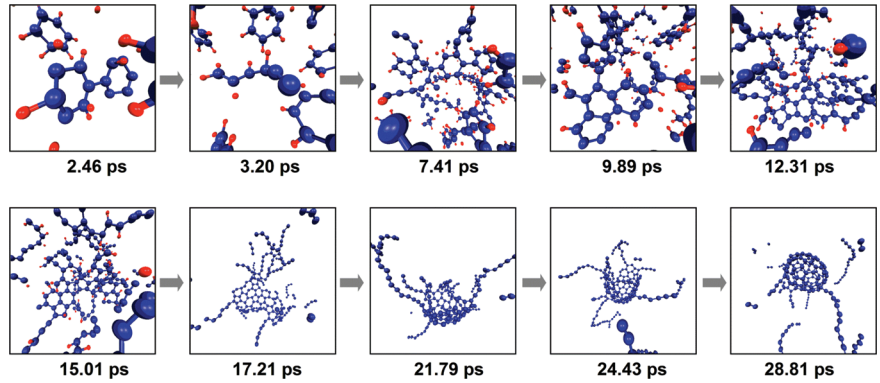

Figure 7. Snapshots from B3000Kg1_1 showing key events. Positions of the carbon and hydrogen atoms are represented by big (blue) and small (red) spheres, respectively.

six-, and seven-membered rings are shown in Figure 6 (5.83, 10.82, and 11.85 ps for B2500Kg1_19) and Figure 7 (3.20 to 15.01 ps). Thus the **first stage** is dominated by *radical creation and ring-opening/fragmentation*. "Healing" of the radical species seems attenuated because of the presence of the volatile hydrogen atoms and only becomes possible when the H/C ratio is further lowered to ~0.33 after the second-time H removal from 10 ps onward. At that stage, we find a maximum in the number of open-chain polyacetylene-like clusters, and a minimum in the number of surviving cyclic rings depending on temperature (30% at $T_n = 2500$ K, and 10% at $T_n = 3000$ K). With cluster growth, the potential energy starts to decrease. This is the **second stage** of formation namely *nucleation of polyacetylene-like clusters*. However, even with the increase in polyacetylene-like cluster size, the number of sp-hybridized carbon atoms is only slowly reduced, and only few five-, six-, and seven-membered rings are formed; Figure 6 (11.85 and 15.01 ps for B2500Kg1_19) and Figure 7 (12.31 and 15.01 ps for B3000Kg1_1) show examples of such. Ring condensation and increase of the fraction of the sp^2-hybridized carbon atoms proceeds to a significant degree *only* when all hydrogen atoms have been removed from the system (after the third time H removal from 15 ps), as shown in Figure 6 (16.79 and 18.08 ps for B2500Kg1_19) and Figure 7 (17.21 and 21.79 ps for B3000Kg1_1). The ring condensation process introduces a significant number of five-membered rings desired to stabilize cluster curvature, as can be seen in Figure 6 (25.67 ps, for B2500Kg1_19) and Figure 7 (for 24.43 ps B3000Kg1_1). Thus the **third stage** is dominated by *ring condensation* process. Finally, "zipper-like" *cage closure*, the **fourth stage** of formation, occurred and is shown in Figure 6 (55.05 ps, for B2500Kg1_19) and Figure 7 (28.81 ps for B3000Kg1_1), when giant fullerenes with 174 C atoms (for B2500Kg1_19) and 120 C atoms (for B3000Kg1_1) are formed. The number of six-membered rings in the growing clusters is always largest, followed by the number of five-membered rings required for stabilizing cage curvature. The number of seven-membered rings is significantly smaller and rarely surpasses 15% of the total number of rings.

Overall, the presence of hydrogen in the system seems to promote C−C bond fragmentation at higher H/C ratios, but also prevents ring condensation at lower H/C ratios. The most striking difference between benzene combustion and pure carbon aggregation then is the fact that the ring condensation process is severely delayed for the former, while it starts nearly immediately after nucleus formation in the case of the latter. In our benzene combustion simulations, the size of the cluster is already nearly determined before the final H removal and consists of a branched network of polyacetylene-like open chains, which only start to condense to a more- or less curved graphene sheet when nearly *all hydrogens* were removed from the system. As a consequence, the borders of the curving graphene clusters have ample time to anneal, perhaps similar to the way Frenklach *et al*. have postulated in a recent work on the migration mechanism of aromatic edge-growth.[55] "Antenna" carbon atoms are thus less likely to be encountered here than in the case of pure carbon, where more C_2 units are continuously added to the "arms of the octopus", as we had called the polyyne chains attached to the growing cage basket structure.[13] At this moment we have not studied and thus cannot comment on the effects a continuous benzene supply might have on these observations.

Another important difference of this combustion simulation, compared with the self-assembly of fullerenes from ensembles of C_2, is the fact that higher temperature (here $T_n = 3000$ K) favors the formation of smaller giant fullerenes, compared to lower temperatures. This can be understood by the devastating effect high temperature has on the vulnerable intermediate radicals. While cluster growth proceeds slower for lower temperatures, it involves more additions of C_6-dimer units that can survive longer than at higher temperatures. Thus, while the polyacetylene-like open-chain cluster growth occurs faster at higher temperatures, the individual fragments constituting the growing cluster are smaller, and their "sticking" probability is lower.

Relationship with Experiment. Our simulation temperatures are higher by about 500 to 1000 K compared to experiment, in an attempt to make our system more reactive and the probability of C−H and C−C bond breaking higher; lower temperatures would require simulation time scales out of reach for our methodology and computer resources. The resulting "take-apart-and-put-together-again" mechanism of disordered PAH growth in our simulations may certainly be somewhat influenced by the choice of high temperature, as the differences between 2500 and 3000 K simulations may indicate. At lower temperature it is expected that the chance of survival of the initial six-membered rings is more likely. However, irregular growth and formation of five-membered rings and seven-membered rings are expected to be more or less the same. We wish to present lower temperature simulations in our next communication. The present choice of high temperature accelerates reactions and growth eventually leading to the formation of fullerene cages within 100 ps, while experimentally this process may take a few milliseconds. Thus in our simulations the residence time is several orders of magnitude shorter compared to experiment.

On the other hand, fullerene cages can be grown in combustions using acetylene[10] as well as benzene,[3] toluene,[8] naphthalene,[36] or 1,2,3,4-tetrahydronapthalene.[6] It is at present unclear whether the presence of six-membered rings in the carbon feedstock is beneficial to the PAH growth process,[6] and as such our observed "take-apart-and-put-together-again"

events bear significance. We are aware that annealing affects are underrepresented in our simulations, but on the other hand, disruptive C-elimination occurring experimentally in form of CO_x formation is also not included in our simulations, and it might be possible that both processes would at least partially neutralize each other as far as PAH growth is concerned.

In experimental fullerene production, the use of an inert carrier gas is required for the fullerene production, and it was shown that the fullerene yield depends on the carrier gas pressure too. In the present model system, no explicit carrier gas atoms were included, but a kinetic energy thermostat takes care of statistical collisions between growing carbon fragments and emulates the effects of the carrier gas in an averaged manner.

An inhibiting effect of hydrogen on carbon cluster growth has been described recently based on experimental observations.[8] This observation was interpreted by postulating a destabilizing effect of hydrogen on intermediate radical species and the mitigation of ring condensation processes due to the hydrogen-occupation at key positions along the polyacetylene-like open chains. Our DFTB/MD simulations corroborate this inhibiting effect and do not indicate a significant amount of thermodynamically preferable maximally conjugated PAH clusters as proposed by Homann and co-workers.[10]

SUMMARY AND CONCLUSIONS

We have performed finite-temperature, nonequilibrium density-functional tight-binding molecular dynamics (DFTB/MD) simulations for the dynamic self-assembly processes of giant fullerene cages during benzene combustion. The DFTB quantum chemical potential energy was benchmarked against first principles B3LYP/6-311G** and *ab initio* G3-type data by Kislov et al.[41] for hydrocarbon species, and agreement was obtained on a similar order of the accuracy of B3LYP/6-311G** itself when compared to G3(MP2,CC)//B3LYP, with nearly negligible difference between noncharge-consistent and self-consistent-charge versions of DFTB. Benzene oxidation was simulated by gradually lowering the H/C ratio due to periodic removal of H atoms from 36 benzene molecules in three stages, covering 1.00, 0.67, 0.33, and 0.00 H/C ratios. The target simulation temperature was set to 2500 and 3000 K, and periodic boundary conditions were applied with liquid benzene-like high initial and subsequent lower carbon densities by variation of the periodic box size. A total of 90 trajectories were run for sometimes up to 225 ps. As in our previous simulations of dynamic fullerene self-assembly from C_2 feedstock,[11−15] we observed no direct assembly of C_{60} buckminsterfullerene. Instead, giant fullerene cages were found with yields slightly higher than for the best pure carbon simulations; for $T_n = 2500$ K, we obtained a yield of 50%, while the fullerenes yield for $T_n = 3000$ K was slightly lower with 42%. More noticeable was the difference in the average cage size; lower simulation temperature favored cages around ~190 carbon atoms, while the higher temperature simulations produced cages around ~160 carbon atoms. The difference is a direct reflection of the intermediate processes, which we found follow a "take-apart-and-put-together-again" pathway; at lower temperatures, cluster growth occurs slower but from larger fragments such as dimer of C_6 species, while at higher temperatures, faster growth occurs from smaller hydrocarbon fragments which are less likely to bind to each other and more frequently fall apart again. Thus, at an intermediate H/C ratio of 0.33 we found that the higher temperature favors larger open-ended polyacetylene-like chains compared to lower temperature simulations, while with no hydrogen present larger giant fullerenes result from the subsequent PAH growth that is somewhat more effective at lower temperatures.

PAH growth only occurs after two-thirds of the hydrogens in the system were removed, and graphene sheet and fullerene growth proceeds only at considerable speed when nearly all hydrogen atoms were removed. Hydrogen is found to have a clear inhibitive effect on PAH and carbon cluster growth in general, in agreement with recent experimental observations.[8] Since the largest cluster is already fully formed when the last hydrogens are removed in our simulations, ring condensation including the incorporation of a significant amount of five-membered rings proceeds until in favorable situations a sufficiently curved graphene basket is formed, which closes in a "zipper-like" fashion with a smaller number of antenna carbon atoms attached to the cage than we had observed for fullerenes grown under conditions of pure carbon species addition.

Most importantly we find a significant amount of sp-hybridized polyyne-like carbon species present up until all hydrogen atoms are removed. The composition of the growing PAH radical species from polyacetylene-like open-chain radical species was found to differ little from the H/C ratio of the system, and no tendency toward formation of maximally condensed PAH systems was observed. As an intermediate result of the "take-apart-and-put-together-again" pathway, we find that a large number of pentagons is directly incorporated in the growing PAHs and subsequent graphene sheets. PAH and subsequent fullerene self-assembly seems to follow a disordered pathway from the opening of the aromatic hydrocarbon feedstock benzene molecules over the aggregation to clusters consisting of linear and branched polyacetylene-like radical open chains, followed by slow ring condensation which becomes faster the more hydrogens are removed from the system. Hence we can say that the fullerene cage may form through four distinct stages (i) radical creation and ring-

opening/fragmentation, (ii) nucleation of polyacetylene-like structures, (iii) ring condensation, and (iv) cage closure. Although we do find that graphene platelets are attaching themselves to growing clusters, our findings stand in remarkable contrast to the hypothesis of ordered PAH platelet growth following thermodynamically most favorable species, and emphasize the necessity to consider growth mechanisms that involve open-chain and pentagon-containing intermediate species in a nonequilibrium environment that allows such structures to play an important role in the cluster growth process.

METHODS

DFTB Quantum Chemical Potential. All QM/MD simulations were performed with the density-functional tight-binding (DFTB) method as implemented in the DFTB program package developed by Frauenheim, Seifert, Elstner, and co-workers.[24,25,56] DFTB is an approximate density functional theory method based on the tight binding approach and uses an optimized minimal Slater-type valence-only basis set in combination with a two-center approximation for Hamiltonian matrix elements. A spin-restricted open-shell formalism was employed where alpha- and beta-electron pairs share the same spatial orbitals. This approach has no problem in describing homolytic bond cleavage, contrary to standard single-reference wave function-based electronic structure methods. To deal with the multiradical open-shell electronic configurations that arise when multiple H atoms are abstracted, and to avoid ionic bond dissociation, we chose to apply a finite Fermi−Dirac electronic temperature T_e to ensure roughly equal population of the radical's singly occupied molecular orbitals MOs (SOMOs). A detailed discussion on the formalism and use of finite electronic temperature within DFTB is given elsewhere.[57] The value of T_e was decided after performing a series of DFTB electronic structure calculations with a range of different T_e choices for multiple phenyl-containing benzene systems. T_e = 5000 K was found to describe the wave function of the neutral radical species correctly, while the use of lower T_e results in a significant number of ionic species that are not penalized in the simple NCC-DFTB formalism.

Molecular Dynamics. To ensure constant density, the calculations were carried out using periodic boundary conditions (PBC) with the gamma-point approximation. All trajectories were computed by calculating analytical DFTB energy gradients on the fly with a Verlet integrator, using 0.48 fs as time integration interval Δt. The Δt of 0.48 fs is shorter by a factor of 2/5 compared with 1.2 fs used in our pure carbon trajectories,[11−15] to ensure proper time integration for the higher frequency C−H stretch vibrations. We found in a benchmark microcanonical NVE simulation that total energy is conserved typically less than 5 kcal/mol for 1.0 ps, which is sufficiently accurate for the purpose of this study. In production calculations, we kept the nuclear temperature T_n constant using scaling of atomic velocities. The scaling is regularly performed after every 4.84 fs, and additionally random scaling is performed with a probability of 10%, thereby an overall scaling probability of 20% applies. Initial velocities were assigned randomly to the benzene molecules. All simulations were performed on a Xeon 2.66 GHz machine, using a sequential algorithm. It takes approximately 24 h wall time for 10340 MD steps with 432 atoms on a single processor.

Acknowledgment. We thank Drs. Viktor Kislov and Alexander Mebel for kindly providing the absolute energies of the G3(MP2,CC) calculations. We also thank Dr. Guishan Zheng and Mr. Shohei Ikoma for the initial geometries of some of our trajectories and Dr. Marcus Lundberg for valuable suggestions regarding the cluster size histograms. B.S. and S.I. acknowledge the Fukui Institute for Fundamental Chemistry for a fellowship, and S.I. acknowledges support by the Program for Improvement of Research Environment for Young Researchers from Special Coordination Funds for Promoting Science and Technology (SCF) commissioned by the Ministry of Education, Culture, Sports, Science and Technology (MEXT) of Japan. This work was in part supported by a CREST (Core Research for Evolutional Science and Technology) grant in the Area of High Performance Computing for Multiscale and Multiphysics Phenomena from the Japan Science and Technology Agency (JST).

Supporting Information Available: A PDF file containing benchmark data of NCC-DFTB and SCC-DFTB energies for 145 hydrocarbon radical compounds, compared to B3LYP/6-311G** and G3(MP2,CC)//B3LYP/6-311G** results, as well as a comparison of B3LYP energies with G3 energies; a collection of typical hydrocarbon species geometries formed after 5 ps at 3000 K; reaction/collision statistics for various carbon fragments during the first 15 ps of simulations at both 2000 and 3000 K temperature; additional carbon type count and ring count statistics for selected successful and unsuccessful trajectories. This material is free of charge *via* the Internet at http://pubs.acs.org.

REFERENCES AND NOTES

1. Kroto, H. W.; Heath, J. R.; O'Brien, S. C.; Curl, R. E.; Smalley, R. E. C_{60}: Buckminsterfullerene. *Nature* **1985**, *318*, 162.
2. Krätschmer, W.; Fostiropoulos, K.; Huffman, D. R. The Infrared and Ultraviolet Absorption Spectra of Laboratory-Produced Carbon Dust: Evidence for the Presence of the C_{60} Molecule. *Chem. Phys. Lett.* **1990**, *170*, 167–170.
3. Howard, J. B.; McKinnon, J. T.; Makarovsky, Y.; Lafleur, A. L.; Johnson, M. E. Fullerenes C_{60} and C_{70} in Flames. *Nature* **1991**, *352*, 139.
4. Hebgen, P.; Goel, A.; Howard, J. B.; Rainey, L. C.; Sande, J. B. V. Synthesis of Fullerenes and Fullerenic Nanostructures in Low-Pressure Benzene/Oxygen Diffusion Flame. *Proc. Combust. Inst.* **2000**, *28*, 1397–1404.
5. Goel, A.; Hebgen, P.; Sande, J. B. V.; Howard, J. B. Combustion Synthesis of Fullerenes and Fullerenic Nanostructures. *Carbon* **2002**, *40*, 177–182.
6. Alford, J. M.; Bernal, C.; Cates, M.; Diener, M. D. Fullerene Production in Sooting Flames from 1,2,3,4-Tetrahydronaphthalene. *Carbon* **2008**, *46*, 1623–1625.
7. *Masters of the Flame: Industrial Production of Fullerenes Becomes a Reality*; Nano-c: Westwood, MA, 2004.
8. Takehara, H.; Fujiwara, M.; Arikawa, M.; Diener, M. D.; Alford, J. M. Experimental Study of Industrial Scale Fullerene Production by Combustion Synthesis. *Carbon* **2005**, *43*, 311–319.
9. Frenklach, M. Reaction Mechanism of Soot Formation in Flames. *Phys. Chem. Chem. Phys.* **2002**, *4*, 2028–2037.
10. Homann, K. H. Fullerenes and Soot Formation—New Pathways to Large Particles in Flames. *Angew. Chem., Int. Ed.* **1998**, *37*, 2434–2451.
11. Irle, S.; Zheng, G.; Elstner, M.; Morokuma, K. From C_2 Molecules to Self-Assembled Fullerenes in Quantum Chemical Molecular Dynamics Simulations. *Nano Lett.* **2003**, *3*, 1657–1664.
12. Zheng, G.; Irle, S.; Morokuma, K. Towards Formation of Buckminsterfullerene C_{60} in Quantum Chemical Molecular Dynamics. *J. Chem. Phys.* **2005**, *122*, 014708/1–7.
13. Irle, S.; Zheng, G.; Wang, Z.; Morokuma, K. The C_{60} Formation Puzzle "Solved": QM/MD Simulations Reveal the Shrinking Hot Giant Road of the Dynamic Fullerene Self-Assembly Mechanism. *J. Phys. Chem. B* **2006**, *110*, 14531–14545.
14. Irle, S.; Zheng, G.; Wang, Z.; Morokuma, K. Theory-Experiment Relationship of the "Shrinking Hot Giant" Road of Dynamic Fullerene Self-Assembly in Hot Carbon Vapor. *Nano* **2007**, *2*, 21–30.

15. Zheng, G.; Wang, Z.; Irle, S.; Morokuma, K. Quantum Chemical Molecular Dynamics Simulations of "Shrinking" of Hot Giant Fullerenes. *J. Nanosci. Nanotechnol.* **2007**, *7*, 1662–1669.
16. Curl, R. F.; Lee, M. K.; Scuseria, G. E. C_{60} Buckminsterfullerene High Yields Unraveled. *J. Phys. Chem. A* **2008**, *112*, 11951–11955.
17. Huang, J. Y.; Ding, F.; Jiao, K.; Yakobson, B. I. Real Time Microscopy, Kinetics, and Mechanism of Giant Fullerene Evaporation. *Phys. Rev. Lett.* **2007**, *99*, 175503/1–4.
18. Jin, C.; Suenaga, K.; Iijima, S. *In Situ* Formation and Structure Tailoring of Carbon Onions by High-Resolution Transmission Electron Microscopy. *J. Phys. Chem. C* **2009**, *113*, 5043–5046.
19. Smalley, R. E. Self-Assembly of the Fullerenes. *Acc. Chem. Res.* **1992**, *25*, 98–105.
20. Ueno, Y.; Saito, S. Geometries, Stabilities, and Reactions of Carbon Clusters: Towards a Microscopic Theory of Fullerene Formation. *Phys. Rev. B* **2008**, *77*, 085403/1–11.
21. Wakabayashi, T.; Achiba, Y. A Model for the C_{60} and C_{70} Growth Mechanism. *Chem. Phys. Lett.* **1992**, *190*, 465–468.
22. Bogana, M.; Ravagnan, L.; Casari, C. S.; Zivelonghi, A.; Baserga, A.; Bassi, A. L.; Bottani, C. E.; Vinati, S.; Salis, E.; Piseri, P.;. *et al*. Leaving the Fullerene Road: Presence and Stability of sp Chains in sp^2 Carbon Clusters and Cluster-Assembled Solids. *New J. Phys.* **2005**, *7*, 1–8.
23. Dunlap, B. I. Accurate Density-Functional Calculations on Large Systems. *Int. J. Quantum Chem.* **1997**, *64*, 193–203.
24. Porezag, D.; Frauenheim, T.; Köhler, C.; Seifert, G.; Kaschner, R. Construction of Tight-Binding-Like Potentials on the Basis of Density-Functional Theory: Application to Carbon. *Phys. Rev. B* **1995**, *51*, 12947–12957.
25. Elstner, M.; Porezag, D.; Jungnickel, G.; Elsner, J.; Haugk, M.; Frauenheim, T.; Suhai, S.; Seifert, G. Self-Consistent-Charge Density-Functional Tight-Binding Method for Simulations of Complex Materials Properties. *Phys. Rev. B* **1998**, *58*, 7260–7268.
26. Zheng, G.; Irle, S.; Morokuma, K. Performance of the DFTB Method in Comparison to DFT and Semiempirical Methods for Geometries and Energies of C_{20} to C_{84} Fullerene Isomers. *Chem. Phys. Lett.* **2005**, *412*, 210–216.
27. Dolgonos, G. A.; Peslherbe, G. H. Calculations of the C_2 Fragmentation Energies of Higher Fullerenes C_{80} and C_{82}. *J. Mol. Model.* **2007**, *13*, 981–986.
28. Zheng, G.; Irle, S.; Elstner, M.; Morokuma, K. Quantum Chemical Molecular Dynamics Study of Fullerene Formation from Open-Ended Carbon Nanotubes. *J. Phys. Chem. A* **2004**, *108*, 3182–3194.
29. Irle, S.; Zheng, G.; Elstner, M.; Morokuma, K. Formation of Fullerene Molecules from Carbon Nanotubes: A Quantum Chemical Molecular Dynamics Study. *Nano Lett.* **2003**, *3*, 465–470.
30. Brenner, D. W. Empirical Potential for Hydrocarbons for Use in Simulating the Chemical Vapor Deposition of Diamond Films. *Phys. Rev. B* **1990**, *42*, 9458–9471.
31. Brenner, D. W. Empirical Potential for Hydrocarbons for Use in Simulating the Chemical Vapor Deposition of Diamond Films. [Erratum to Document Cited in CA114(6): 53045x]. *Phys. Rev. B* **1992**, *46*, 1948.
32. Brenner, D. W. The Art and Science of an Analytical Potential. *Phys. Stat. Sol. B* **2000**, *217*, 23–40.
33. Yamaguchi, Y.; Maruyama, S. A Molecular Dynamics Simulation of the Fullerene Formation Process. *Chem. Phys. Lett.* **1998**, *286*, 336–342.
34. Yamaguchi, Y.; Colombo, L.; Piseri, P.; Ravagnan, L.; Milani, P. Growth of sp-sp^2 Nanostructures in a Carbon Plasma. *Phys. Rev. B* **2007**, *76*, 134119/1–7.
35. Pope, C. J.; Marr, J. A.; Howard, J. B. Chemistry of Fullerenes C_{60} and C_{70} Formation in Flames. *J. Phys. Chem.* **1993**, *97*, 11001–11013.
36. Ahrens, J.; Bachmann, M.; Baum, T.; Griesheimer, J.; Kovacs, R.; Weilmünster, P.; Homann, K. H. Fullerenes and Their Ions in Hydrocarbon Flames. *Int. J. Mass Spectrosc. Ion Proc.* **1994**, *138*, 133–148.
37. Grieco, W. J.; Lafleur, A. L.; Swallow, K. C.; Richter, H.; Taghizadeh, K.; Howard, J. B. In *Fullerenes and PAH in Low-Pressure Premixed Benzene/Oxygen Flames*; 27th Symposium (International) on Combustion, 1998; The Combusition Institute: 1998; pp 1669−1675.
38. Grieco, W. J.; Howard, J. B.; Rainey, L. C.; Sande, J. B. V. Fullerenic Carbon in Combustion-Generated Soot. *Carbon* **2000**, *38*, 597–614.
39. Cavallotti, C.; Mancarella, S.; Rota, R.; Carra, S. Conversion of C_5 into C_6 Cyclic Species through the Formation of C_7 Intermediates. *J. Phys. Chem. A* **2007**, *111*, 3959–3969.
40. Kislov, V. V.; Mebel, A. M. Ab Initio G3-type/Statistical Theory Study of the Formation of Indene in Combustion Flames. I. Pathways Involving Benzene and Phenyl Radical. *J. Phys. Chem. A* **2007**, *111*, 3922–3931.
41. Kislov, V. V.; Mebel, A. M. An Ab Initio G3-Type/Statistical Theory Study of the Formation of Indene in Combustion Flames. II. The Pathways Originating from Reactions of Cyclic C_5 Species—Cyclopentadiene and Cyclopentadienyl Radicals. *J. Phys. Chem. A* **2008**, *112*, 700–716.
42. Violi, A.; Venkatnathan, A. Combustion-Generated Nanoparticles Produced in a Benzene Flame: A Multiscale Approach. *J. Chem. Phys.* **2006**, *125*, 054302/1–054302/8.
43. Richter, H.; Benish, T. G.; Mazyar, O. A.; Green, W. H.; Howard, J. B. Formation of Polycyclic Aromatic Hydrocarbons and Their Radicals in a Nearly Sooting Premixed Benzene Flame. *Proc. Comb. Inst.* **2000**, *28*, 2609–2618.
44. Richter, H.; Mazyar, O. A.; Sumathi, R.; green, W. H.; Howard, J. B.; Bozzelli, J. W. Detailed Kinetic Study of the Growth of Small Polycyclic Aromatic Hydrocarbons 1. 1-Naphthyl + Ethyne. *J. Phys. Chem. A* **2001**, *105*, 1561–1573.
45. Richter, H.; Howard, J. B. Formation and Consumption of Single Ring Aromatic Hydrocarbons and Their Precursors in Premixed Acetylene, Ethylene, and Benzene Flames. *Phys. Chem. Chem. Phys.* **2002**, *4*, 2038–2055.
46. Uc, V. H.; Alvarez-Idaboy, J. R.; Galano, A.; Garcia-Cruz, I.; Vivier-Bunge, A. Theoretical Determination of the Rate Constant for OH Hydrogen Abstraction from Toluene. *J. Phys. Chem. A* **2006**, *110*, 10155–10162.
47. Chenoweth, K.; van Duin, A. C. T.; Goddard, W. A., III. ReaxFF Reactive Force Field for Molecular Dynamics Simulations of Hydrocarbon Oxidation. *J. Phys. Chem. A* **2008**, *112*, 1040–1053.
48. Otte, N.; Scholten, M.; Thiel, W. Looking at Self-Consistent-Charge Density Functional Tight Binding from a Semiempirical Perspective. *J. Phys. Chem. A* **2007**, *111*, 5751–5755.
49. Rabuck, A. D.; Scuseria, G. E. Improving Self-Consistent Field Convergence by Varying Occupation Numbers. *J. Chem. Phys.* **1999**, *110*, 695–700.
50. DiNaro, J. L.; Howard, J. B.; Green, W. H.; Tester, J. W.; Bozzelli, J. W. Elementary Reaction Mechanism for Benzene Oxidation in Supercritical Water. *J. Phys. Chem. A* **2000**, *104*, 10576–10586.
51. Alfè, M.; Apicella, B.; Barbella, R.; Tregrossi, T.; Ciajolo, A. Similarities and Dissimilarities in *n*-Hexane and Benzene Sooting Premixed Flames. *Proc. Comb. Inst.* **2007**, *31*, 585–591.
52. Yang, B.; Li, Y.; Wei, L.; Huang, C.; Wang, J.; Tian, Z.; Yang, R.; Sheng, L.; Zhang, Y.; Qi, F. An Experimental Study of the Premixed Benzene/Oxygen/Argon Flame with Tunable Synchrotron Photoionization. *Proc. Comb. Inst.* **2007**, *31*, 555–563.
53. Bittner, J. D.; Howard, J. B. Composition Profiles and Reaction Mechanisms in a Near-Sooting Premixed Benzene/Oxygen/Argon Flame. *Proc. Comb. Inst.* **1981**, *18*, 1105–1116.
54. Defoeux, F.; Dias, V.; Renard, C.; Tiggelen, P. J. V.; Vandooren, J. Experimental Investigation of the Structure of a Sooting Premixed Benzene/Oxygen/Argon Flame Burning at Low Pressure. *Proc. Combust. Inst.* **2005**, *30*, 1407–1415.

55. Frenklach, M.; Schuetz, C. A.; Ping, J. Migration Mechanism of Aromatic-Edge Growth. *Proc. Combust. Inst.* **2005**, *30*, 138–1396.
56. Seifert, G.; Porezag, D.; Frauenheim, T. Calculations of Molecules, Clusters, and Solids with a Simplified LCAO-DFT-LDA Scheme. *Int. J. Quantum Chem.* **1996**, *58*, 185–192.
57. Ohta, Y.; Okamoto, Y.; Irle, S.; Morokuma, K. Rapid Growth of a Single-Walled Carbon Nanotube on an Iron Cluster: Density-Functional Tight-Binding Moleculer Dynamics Simulations. *ACS Nano* **2008**, *2*, 1437–1444.